

Flow in Compliant Tubes: Control and Stabilization by Multilayered Coatings

Natalya Kizilova^a, Mahmoud Hamadiche^b, and Mohamed Gad-el-Hak^c

^aDepartment of Theoretical Mechanics, Kharkov National University, Svobody Sq. 4, 61195 Kharkov, Ukraine, e-mail: nnk_@bk.ru

^bLaboratoire de Mécanique des Fluides et d'Acoustique, Ecole Centrale de Lyon, 36 Av. Guy de Collongue, UMR5509, F 69134 Ecully, France, e-mail: mahmoud.hamadiche@ec-lyon.fr

^cDepartment of Mechanical Engineering, Virginia Commonwealth University, Richmond, VA 23284-3015, e-mail: gadelhak@vcu.edu

Abstract

Flow instability and flow control in compliant tubes are studied in application to biological systems and technical devices. Common features of the flows are determined by fluid–structure interaction that may lead to absolute and convective instabilities. The stability of a steady flow of an incompressible viscous fluid through a compliant tube composed of three anisotropic viscoelastic layers with different material properties is studied. The eigenvalues of the system are calculated for the no-stress and no-displacement boundary conditions at the outer surface of the tube. It is shown that the flow can be stabilized by a proper choice of the thickness, viscosity and elastic moduli of the layers. The multilayered viscoelastic coatings can be used to control flows in compliant ducts.

1. INTRODUCTION

Biofluid flows in distensible tubes, fluid–structure interaction and flow-induced instabilities are the subject of many review papers [1–3]. Currently new results have been obtained both in theory and experiment, and new important aspects of the fluid–structure interaction have been found in different biofluid-conveying ducts including blood flow in blood vessels, air flow in human's airways, peristaltic transport in collapsible elements of the gastrointestinal tract, urine in the urethra, tears in the tear ducts, milk in the milk ducts. In each of these cases, the ducts are composed of more than one layer each with different material parameters. Flow instability in compliant ducts can produce flow-limitation and pressure-limitation effects, wall oscillations, damage of the innermost layer (endothelium) of the duct, and sound generation in veins, airways, larynx and glottis. Many problems of blood flow through stents and grafts, collapse of airways and apnea in snorers, speech generation, and others are determined by the flow interaction with compliant walls and the stability of the combined system. Therefore, keen understanding of the mechanics of those instabilities and particularly their control is desired.

The very first result on a fluid flow through distensible tubes was published by Conrad [4], although experimental observations of wall oscillations of the equine carotid artery have been made by Antonio Valsalva as early as 1824. French physician Jean Louis Marie Poiseuille carried out a series of in vitro experiments with blood flow in the distensible arterial segments and discovered the relationship between the flow rate Q and the driving pressure drop δP . When the tube conveying a fluid is flexible, strong couplings exist between the fluid flow through the tube, the driving pressure drop δP , the external pressure P_{ext} , and the shape of the tube cross-section determining the flow boundary. When the pressure P_{int} inside the tube is no less than P_{ext} , the tube is either fully open or dilated and coupling is weak, but it is strong when the tube collapses to elliptic cross-section and further to a contact between the opposite sides of the wall and a full collapse. The collapse state is characterized by some unusual and physiologically important phenomena, including flow limitation and self-excited oscillations [5]. When the tube is not collapsed, the flow influences the wall motion and vice versa, and the energy transfer at the fluid–solid interface produces some phenomena connected with absolute and convective instability of the system.

Liquid flows through compliant tubes in technological and biomedical processes, for example fluid separation, drug purification, polymer processing, blood oxygenation in pump oxygenators, often creates turbulent boundary layers, which in turn can lead to significant loss in efficiency. Turbulent skin

friction is responsible for a significant portion of the drag experienced by aircraft, ships and underwater vehicles. In water and wind tunnels, the methods of delaying laminar-to-turbulence transition, skin-friction drag reduction in the turbulent flows, quelling vibrations, and suppressing the flow-induced noise are promising for different applications [6]. Fluid flow accompanied by wall oscillations and fluid stirring is essential in heat transfer processes (water heating and distribution, steam generating stations, petroleum industries, nuclear power stations) because the flow instability influences the heat transfer rates [7].

An avalanche of the experimental and theoretical investigations of the flow stabilization by a compliant surface had been promoted by observations of the swimming dolphins. Kramer was the first who suggested a dolphin's body experiences low drag due to special structure of its compliant skin, which allows delaying transition to turbulence and maintaining the laminar flow [8]. Recent successes in the field of composite materials lead to elaboration of promising coatings for turbulent boundary layer stabilization and laminar-to-turbulence transition postponement [9–13]. It is established that a sufficiently compliant coating can completely suppress Tollmien–Schlichting waves, giving a significant delay in the onset of laminar-to-turbulent transition mostly for flat-plate boundary layers [6, 9, 11–15]. Unfortunately, other types of solid-based modes can also become unstable, and the problem of finding the material parameters for a successful coating for practical use is difficult [16, 17–22]. Noticeable success has been achieved in studying and mimicking the detailed inner structure and lubrication of dolphin's skin, which is important for elaboration of the compliant coatings for the underwater vehicles [23]. The results of detailed FEM computations of the flow past the dolphin's fin taking into account realistic morphological structure of the papillary layer are presented in [24]. It was shown the skin structure allows the flow-skin interface to behave similar to an anisotropic compliant wall in regions of favorable and adverse pressure gradients acting on the fin. In that way anisotropic composite materials are more promising as candidates for the successful coatings than the isotropic ones.

Certain two-layer compliant coatings composed by an outer isotropic elastic layer with or without applied longitudinal tension mounted onto the inner anisotropic elastic foundation have been proposed [25, 26] for the drag reduction. Since the parameters of the successful coating that locally reduce the growth of disturbances depend strongly on the Reynolds number, the multi-panel coating in which each plane is optimized for a particular Reynolds number range can be advantageous for practice. That sort of the multilayered compliant coating consisting of two isotropic panels in series has been proposed for delay of laminar-turbulent transition [15]. Anisotropy of the compliant Kramer-type coating has also been found important for the flow stabilization [14, 26, 27]. When anisotropic materials are used for the layers and the set of material parameters is enriched by different Young's moduli, Poisson ratios and shear moduli, the flow control by a proper choice of the wall parameters becomes even easier [21, 22].

The advantages of the three-layer coating accounting for the viscosity of the wall layers have been studied in [20, 21, 28, 29]. It was shown, the fluid flow in the three-layer tube could be stabilized by variations of the elasticity of the inner and outer layer or viscosity of the middle layer depending on the boundary conditions at the outer surface of the tube. The most-unstable fluid-based mode could be stabilized and in some cases even the absolute instability could be eliminated [22]. The parameters of different coatings that stabilize the system, prevent flow separation and skin drag growth, delay the laminar-turbulent transition, suppress the self-excited oscillations and noise generation can be used for the passive control over the flow in the ducts and over the surfaces. In this paper, control mechanisms of biofluid flow stability are discussed, and passive control of the flow stability in multilayered tubes at different boundary conditions is substantiated.

2. FLOW CONTROL

The problem of flow control is important for fluid flow in compliant tubes for both biological and technical systems. Reactive control in living beings is provided by a proper variation of rheological properties and geometry of the solid and viscosity and velocity of the fluid. The nervous and humoral systems are responsible for the reactive control as well as the local chemical and mechanical stimuli. For instance, thickness and rigidity of the blood vessel walls and the lumen of the vessel can be changed by contraction of the smooth muscle cells composing the middle layer of the wall. The muscle contraction is determined by the hydrostatic pressure in the blood vessel and the shear rate at the inner (epithelial) layer composed by mechanosensitive cells.

The cells of the inner layer control also the growth and formation of the vascular network, providing

optimal branching angles in the bifurcations [30]. The mechanism of formation of the optimal branching networks that supply the inner organs and muscles and distribute oxygen and nutrients to each cell at minimal total energy expenses is based on the long-term reactive control of the lumens of the vessels forming the bifurcations in a growing living body. If the shear rate at the wall is maintained by the mechanosensitive cells within certain narrow physiological limits, the relationship between the flow rate and diameter of the tube becomes close to $Q \sim d^3$ and the flow continuity condition in the bifurcation gives $d_0^3 = d_1^3 + d_2^3$, where d_0 and $d_{1,2}$ are diameters of the parent and daughter vessels accordingly. The validity of the relationship has been confirmed by numerous observations in mammalian circulatory systems, fluid and gas transport systems of fishes and insects, trophic fluid transport systems of a variety of suspension-feeding marine invertebrates (mollusks, brachiopods, lophophore, sponges) [31], the conducting systems of plant leaves [32–34], tree branching [35] and even in the bifurcations of axons [36] which are also formed by compliant membranes filled with viscous intercellular contents of the nervous cell. The identity of the branching laws in animals and plants confirms that similar principles of the reactive flow control in the living nature had been developed during the evolution. A reactive response of the vessel wall geometry and material properties to the altered flow parameters determines development of different pathology as well. Initial intimal thickening, fibrosis, smooth muscle hypertrophy and fat accumulation in the vessel wall and plaque formation are strongly influenced by the flow conditions [37, 38].

As surgeons have observed it, when a blood vessel is dissected at the bifurcation, the blood jet subtends the same angle with the axis of the parent vessel as the daughter vessel had before dissection. Consequently, the branching angles correspond to the jet flows and provide minimal shear stress at the inner walls of the daughter vessels near the bifurcation. If the branching angle is perturbed by any developmental abnormalities or pathology and became less/greater than the optimal angle, the shear stress will exceed the optimal value at the outer/inner surface and will be reduced at the inner/outer surface of the daughter vessel [34]. The signal about the nonuniform stress distribution at the inner and outer walls will be transferred by the mechanoreceptors into the other layers of the blood vessels providing their adequate non-uniform growth and gradual correction of the perturbed branching angles towards their optimal values.

The vascular regions near the bifurcations are the most vulnerable for the atherosclerotic plaque formation, because flow separation after the bifurcation, nonuniform stress distribution and slow blood flow in the stagnation regions are favorable for developing different pathology of the blood vessel wall [39, 40]. Examples of the reactive control of the fluid flow and solid transformations (normal and pathological growth, degeneration, ageing variations) can be found everywhere in the living bodies. Preventing the flow separation is also important in the technical applications giving the substantial reduction in the form drag and lift enhancement [41].

Passive flow control is widely used in medicine, especially in the cardiovascular surgery. Powerful computational fluid dynamics technique allows detailed computations of the blood flow profiles and stress distribution at the inner surface of the vascular bifurcations with complex geometry, arterial stenosis and aneurisms, and heart chambers. In theory, the optimal shape of the bifurcations (i.e. carotid sinus, aortic bifurcation) can be computed to avoid significant flow separation and extensive stagnation regions. The optimal branching angles of the arterial and arteriovenous grafts can also be computed to prevent flow instability and wall vibrations and provide optimal propagation and reflection of the blood pressure waves [42]. Unfortunately, more than half of the arteriovenous grafts fail and require surgical reconstruction [43] as well as in some several months the stented vessels could become occluded again due to intimal growth.

Active control over the blood flow regimes (Reynolds number), blood pressure, heat and mass exchange at the vessel wall and in the capillaries, flow pumping by the contracting muscles, flow stabilization, delaying laminar-turbulent transition, suppression of vibrations of the solid are also important in medicine. Blood viscosity, wall distensibility, vessel lumen, hydrostatic pressure, blood ejection by the heart and some other parameters can be modified and kept at certain values by chemicals, mechanical and electrical forces. Since a wide range of Reynolds numbers from $Re = 10^{-3}$ in capillaries to $Re \approx 6000$ in the aorta is observed, the problem of the passive, active and reactive control of the blood flow in the vessels remains topical for the biomedical applications.

In the present paper some novel results on the flow instability in the multilayered viscoelastic tubes are reported and a possibility to stabilize the flow and in that way control the flow stability at different boundary conditions is substantiated.

3. PROBLEM FORMULATION

The stability of the Poiseuille flow of a viscous incompressible fluid in a multilayered thick-walled viscoelastic tube has been studied by Hamadiche and Kizilova [20] for the no-displacement boundary conditions at the outer surface of the wall. In this paper the flow of the viscous liquid through a long viscoelastic thick-walled tube with the inner radius R , thickness h and length L is considered at different boundary conditions. The wall is composed of three anisotropic layers with thicknesses h_1, h_2, h_3 , where $h_1 + h_2 + h_3 = h$. The conservation equations for the fluid are the incompressible Navier-Stokes equations

$$\nabla \cdot \vec{v} = 0 \quad (1a)$$

$$\frac{\partial \vec{v}}{\partial t} + \vec{v} \cdot \nabla \vec{v} = -\frac{1}{\rho_f} \nabla p + \frac{1}{\rho_f} \nabla \cdot \hat{\sigma} \quad (1b)$$

and the mass and momentum conservation equations for the incompressible wall are

$$\begin{aligned} \nabla \cdot \vec{u}^{(j)} &= 0 \\ \rho_w^{(j)} \frac{\partial^2 \vec{u}^{(j)}}{\partial t^2} &= -\nabla p^{(j)} + \nabla \cdot \hat{\sigma}^{(j)} \end{aligned} \quad (2)$$

where \vec{v} is the flow velocity, $\vec{u}^{(j)}$ is the wall displacement, ρ_f and $\rho_w^{(j)}$ are the mass densities for the fluid and solid layers, $j = 1, 2, 3$ is the number of the layer, p and $p^{(j)}$ are the hydrostatic pressures, $\hat{\sigma}$ and $\hat{\sigma}^{(j)}$ are the stress tensors for the fluid and the wall layers.

The viscoelastic body with parallel connection of the elastic and viscous properties (Voight model) has been considered for the solid layers

$$\sigma_i^{(j)} = A_{ik}^{(j)} \varepsilon_k^{(j)} + \mu_w^{(j)} \frac{\partial}{\partial t} \varepsilon_k^{(j)} \quad (3)$$

where $A_{ik}^{(j)}$ is the matrix of elasticity coefficients, $\mu_w^{(j)}$ are the viscosities of the layers, $\varepsilon_{ik}^{(j)} = \frac{1}{2} (\nabla_i u_k^{(j)} + \nabla_k u_i^{(j)})$ is the strain tensor, $\vec{\sigma}^{(j)} = \{\sigma_{11}^{(j)}, \sigma_{22}^{(j)}, \sigma_{33}^{(j)}, \sigma_{23}^{(j)}, \sigma_{13}^{(j)}, \sigma_{12}^{(j)}\}$ is the stress vector, and $\vec{\varepsilon}^{(j)}$ is the similar strain vector.

The boundary conditions include the continuity conditions for the fluid velocity and displacement of the inner layer and normal and tangential stresses at the fluid–solid interface; the continuity conditions for the displacements and stresses at the interfaces of the layers respectively:

$$r = R : \vec{v} = \frac{d\vec{u}^{(1)}}{dt}, \quad \vec{\sigma}_n = \vec{\sigma}_n^1, \quad \vec{\sigma}_\tau = \vec{\sigma}_\tau^1 \quad (4)$$

$$r = R + h_1 : \vec{u}^{(1)} = \vec{u}^{(2)}, \quad \vec{\sigma}_n^1 = \vec{\sigma}_n^2, \quad \vec{\sigma}_\tau^1 = \vec{\sigma}_\tau^2 \quad (5)$$

$$r = R + h_1 + h_2 : \vec{u}^{(2)} = \vec{u}^{(3)}, \quad \vec{\sigma}_n^2 = \vec{\sigma}_n^3, \quad \vec{\sigma}_\tau^2 = \vec{\sigma}_\tau^3 \quad (6)$$

At the outer surface of the tube both no-stress

$$r = R + h : \vec{\sigma}_n^3 = 0, \quad \vec{\sigma}_\tau^3 = 0 \quad (7)$$

and no-displacement

$$r = R + h : \vec{u}^{(3)} = 0 \quad (8)$$

boundary conditions have been considered, where n and τ denotes the normal and tangential components of the stress tensor.

The solution of the fluid–structure interaction problems (1)–(7) and (1)–(6), (8) has been found as a superposition of the steady liquid flow and small axisymmetric disturbance in the form of the normal mode:

$$\begin{aligned} \{\bar{v}, p\} &= \{\bar{v}^*, p^*\} + \{\bar{v}^\circ, p^\circ\} \cdot \exp(st + ikz + in\theta) \\ \{\bar{u}^{(j)}, p^{(j)}\} &= \{\bar{u}^{(j)*}, p^{(j)*}\} + \{\bar{u}^{(j)\circ}, p^{(j)\circ}\} \cdot \exp(st + ikz + in\theta) \end{aligned} \tag{9}$$

where $\bar{v}^\circ, \bar{u}^{(j)\circ}, p^\circ, p^{(j)\circ}$ are the amplitudes of the corresponding disturbances, $k = k_r + ik_i, s = s_r + is_i, s_i$ is the wave frequency, k_r is the wavenumber, s_r and k_i are spatial and temporal amplification rates. The steady part $\{\bar{v}^*, p^*\}$ of (9) is identified with Poiseuille flow. Both isotropic and transversely isotropic materials for the wall layers have been studied.

According to the experimental data [44, 45] the plane of isotropy of each layer is perpendicular to the radial axis and the matrix of elasticity coefficients is the following:

$$\left(A_{ik}^{(j)} \right)^{-1} = \begin{pmatrix} (E_2^{(j)})^{-1} & -\nu_2^{(j)}(E_2^{(j)})^{-1} & -\nu_2^{(j)}(E_2^{(j)})^{-1} & 0 & 0 & 0 \\ -\nu_2^{(j)}(E_2^{(j)})^{-1} & (E_1^{(j)})^{-1} & -\nu_1^{(j)}(E_1^{(j)})^{-1} & 0 & 0 & 0 \\ -\nu_2^{(j)}(E_2^{(j)})^{-1} & -\nu_1^{(j)}(E_1^{(j)})^{-1} & (E_1^{(j)})^{-1} & 0 & 0 & 0 \\ 0 & 0 & 0 & (G_2^{(j)})^{-1} & 0 & 0 \\ 0 & 0 & 0 & 0 & (G_1^{(j)})^{-1} & 0 \\ 0 & 0 & 0 & 0 & 0 & (G_1^{(j)})^{-1} \end{pmatrix} \tag{10}$$

where $G_{1,2}^{(j)}$ are the shear modules, $E_{1,2}^{(j)}$ are the Young’s modules and $\nu_{1,2}^{(j)}$ are the Poisson ratios of the layers. The values $E_{1,2}^{(j)}$ and $G_{1,2}^{(j)}$ are different for different blood vessels (of elastic or muscle type) and for the normal vessel wall and at some pathological cases including hypertension, atherosclerosis and hyperlipidemia. The values $\nu_{1,2}^{(j)}$ for the incompressible materials are close to zero. Since the blood vessel walls are filled with small vessels delivering the blood into the wall (vasa vasorum), some compressibility of the wall material can also be taken into account. The tubes of different technical devices composed from several layers with different viscoelastic parameters can also be considered basing on (1)–(8).

The temporal and spatial eigenvalues of the systems (1)–(7) and (1)–(6), (8) have been computed using the technique described in [18, 19, 22].

The problems have a large number of the parameters, so we concentrated on the effect of the Reynolds number, viscous and elastic parameters and thicknesses of the wall layers on the system stability for axisymmetric disturbances ($n=0$ in (9)).

4. RESULTS AND DISCUSSIONS

The temporal eigenvalues of the system in the complex (s_i, s_r) -plane are shown in Fig. 1a. The modes located near the real axis of the (s_i, s_r) -plane are solid based and those located near the imaginary axis are fluid based. The modes near the point of origin couple efficiently the solid and fluid motion. The distribution density of the eigenvalues along the real and imaginary axis depends on the elastic and fluid inertia forces determined by the values Γ and Re . For the cylindrical water column with free boundaries the fluid based modes only remain in the (s_i, s_r) -plane, whereas for the empty viscoelastic shell the fluid based modes disappear and we can find the solid based ones only. The modes involved efficiently in the fluid–solid interaction are placed near the origin of the complex plane where the unique unstable mode with $s_r > 0$ is located.

Unless indicated otherwise, the numerical values of the nondimensional physical parameters are as follows: the wavenumber $k_r = 2.5$, the frequency $s_i = 2$, the Reynolds number $Re=100$, the ratio of the fluid inertia to elastic forces $\Gamma = 1$, the non-dimensional Young’s modulus and shear modulus are $\Xi_{1,2}^{(j)} = 1$ and $\Theta_{1,2}^{(j)} = 3$, the solid to fluid density ratio $\rho^{(j)} = \rho_w^{(j)}/\rho_f$ is $\rho^{(j)} = 1$, the relative (nondimensional) solid to fluid viscosity of the layers is $\mu^{(j)} = \mu_w^{(j)}/\mu_f$, the non-dimensional tube radius and the thicknesses of the layers are $R = 1, H = 0.1, H_1 = 0.02, H_2 = 0.04, H_3 = 0.04$. The calculated results have been found to be practically insensitive to the Poisson’s ratio of the layers.

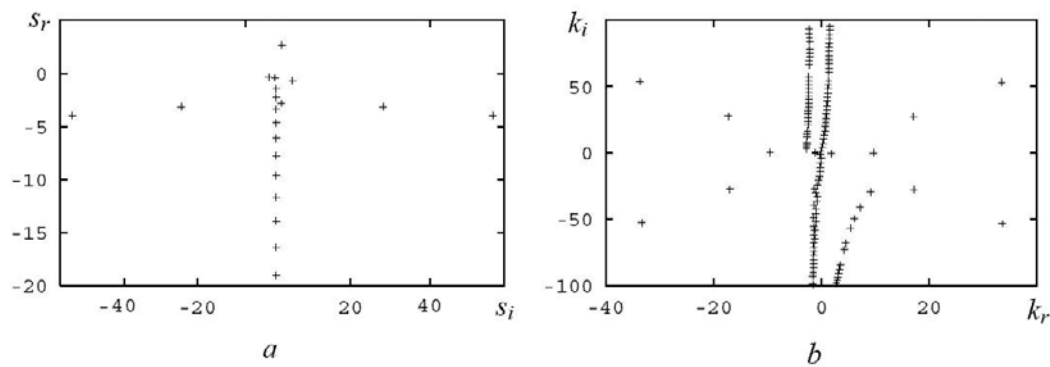


Figure 1. Temporal (a) and spatial (b) eigenvalues of the system at the no-stress conditions for the material parameters presented in the text.

The spatial eigenvalues of the system in the (k_r, k_i) -plane are plotted in Fig. 1b. The spectrum in the complex wavenumber plane forms four branches in the upper part ($k_i > 0$) of the plane and four branches in its lower part ($k_i < 0$). The modes in the upper part are the monochromatic components of the solution for $z > 0$. In other words, they are solutions in the region located behind (downstream) the source of perturbations. The modes in the lower part of the (k_r, k_i) -plane correspond to the solutions located upstream the source of perturbations. Superposition of the forward and backward propagating waves produces a complicated pattern of the pressure and flow time variation in the fluid and the wall oscillations in any given cross section of the tube.

When the no-displacement boundary conditions are applied at the outer surface of the tube, the temporal Eigen modes in (s_r, s_i) -plane form five branches (Fig. 2a). The four horizontal branches are composed of the solid based modes and the vertical one is composed of the fluid based modes. The four branches in the (k_r, k_i) -plane in Fig. 2b correspond to the upstream and downstream propagating torsional and flexural modes. The spatial eigenvalues at the no-displacement conditions form the more complex pattern because the flow-induced wall displacement is constrained by the attachment conditions at the outer surface of the tube that enhances the fluid–solid interaction. At the no-stress conditions the wall may be efficiently involved into the motion produced by pressure wave propagation in the fluid depending on the wall elasticity only. Nevertheless it is not clear which mode actually exists for given boundary conditions, investigation of the system stabilization by decreasing the instability or elimination of the most-unstable mode provides an efficient tool for understanding the mechanism of stabilization.

When the outer surface of the tube is free and the wall displacement is entirely defined by the fluid flow and wall parameters, the eigenvalues of the system are mainly the fluid based. Contrary to the case, the eigenvalues are mainly the solid based when the wall is attached to the rigid surrounding

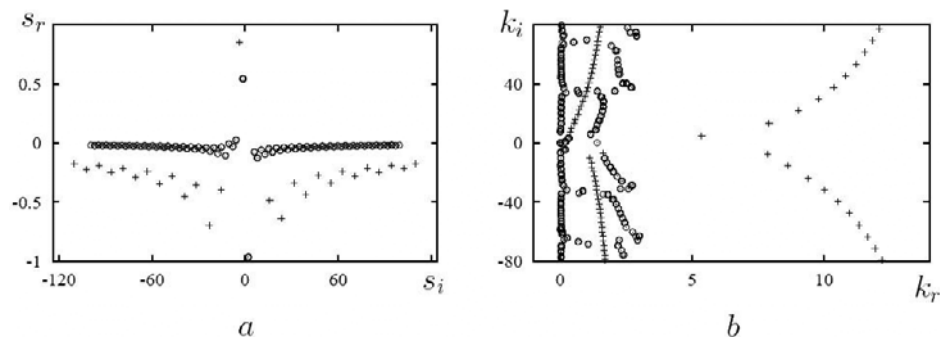


Figure 2. Comparison between isotropic and anisotropic eigenvalues, for the no-displacement boundary conditions. +: isotropic layers, $\Theta^{(l)} = 1$, $\Xi^{(l)} = 2$; o: anisotropic layers, $\Theta_1^{(l)} = 0.1$, $\nu_{12}^{(l)} = 0.1$, $\Theta_2^{(l)} = 1$, $\Xi_1^{(l)} = 20$, $\Xi_2^{(l)} = 2$. (a) Temporal eigenvalues of three-layer viscoelastic tube in the (s_r, s_i) -plane. (b) Spatial eigenvalues of three-layer viscoelastic tube in the (k_r, k_i) -plane.

medium [20]. In comparison with solution of the problem for the no-displacement boundary conditions (Figs. 2a, b) the spatial eigenvalues of the system at the no-stress conditions also form less complex pattern (Figs. 1a, b). In both cases one can find a few branches for the long waves and one more branch for the relatively short waves ($k_r = 10 - 20$ and $k_r = 5 - 10$ for the no-stress and no-displacement boundary conditions accordingly). The bigger values for both long and short waves are proper to the no-displacement case. The set of the modes for the long waves at the no-displacement conditions is more various and there is some difference between the modes for the isotropic and anisotropic walls (Figs. 2a, b).

The dependence of the temporal amplification rate on the wavenumber has been calculated in an effort to establish the functional relationship between the temporal and spatial modes. The corresponding dependence for several values of the Reynolds number is plotted in Fig. 3a. For the low Reynolds numbers regime there is a wide range of unstable modes ($s_r > 0$) including short waves. For the high Reynolds numbers the instability is limited by the long waves only ($k_r < 8$). Note that the amplification rate of the unstable mode reaches its upper limit with increasing the Reynolds number. As it is presented in Fig. 3a, the amplification rate reaches its maximum value when the system is in its most amplified mode.

In [20, 21] the effect of the rheological parameters of the wall layers on the system stability has been studied and some opportunities for stability control and elimination of the absolute instability have been found. Extensive numerical computations at no-stress boundary conditions for different material parameters have revealed that both temporal amplification rate and group velocity are also influenced by the wall rigidity and viscosity. The dependence of the temporal amplification rate of the most-unstable mode on the shear modulus of one of the layer while the shear modulus of the two other layers remains unchangeable is plotted in Fig. 3b. In the considered variation range of $\Theta_1^{(j)}$ and $\Theta_2^{(j)}$ one can see that an increase in the shear modulus of the three layers simultaneously leads to an increase in the amplification rate, as is indicated by the solid line in Fig. 3b. An increase in the shear modulus $\Theta_1^{(1)} = \Theta_2^{(1)}$ of the inner layer which is in contact with fluid while the shear modulus of the other layers are $\Theta_1^{(2)} = \Theta_1^{(3)} = \Theta_2^{(2)} = \Theta_2^{(3)} = 1$ leads to noticeable decrease in the temporal amplification rate down to its negative values $s_r < 0$ that corresponds to the temporal stability of the system as it is indicated by the curve 2 in Fig. 3b. At sufficiently large values $\Theta_1^{(1)} = \Theta_2^{(1)} > 7$, the system becomes stable. An increase in the shear modulus $\Theta_1^{(2)} = \Theta_2^{(2)}$ or $\Theta_1^{(3)} = \Theta_2^{(3)}$, while the parameters of the other layers are held $\Theta_1^{(1,3)} = \Theta_2^{(1,3)} = 1$ or $\Theta_1^{(1,2)} = \Theta_2^{(1,2)} = 1$, stabilizes the system as is indicated by curves 3–4 in Fig. 3b. The obtained result corresponds to experimental and theoretical considerations on the flow instability over the compliant surface. The results presented in Fig. 3b reveal that flow stabilization in the complied tube can be achieved by using the relatively rigid inner coating (inner layer) of certain thickness.

The effect of the viscosity of each layer on the temporal amplification rate has also been examined by numerical calculations. The dependence of the temporal amplification rate on the viscosity of one of the layer while other layers are non-viscous (elastic) is shown in Fig. 4a for the isotropic layers and the no-stress conditions at the outer surface of the tube. An increase in the viscosity of the second and

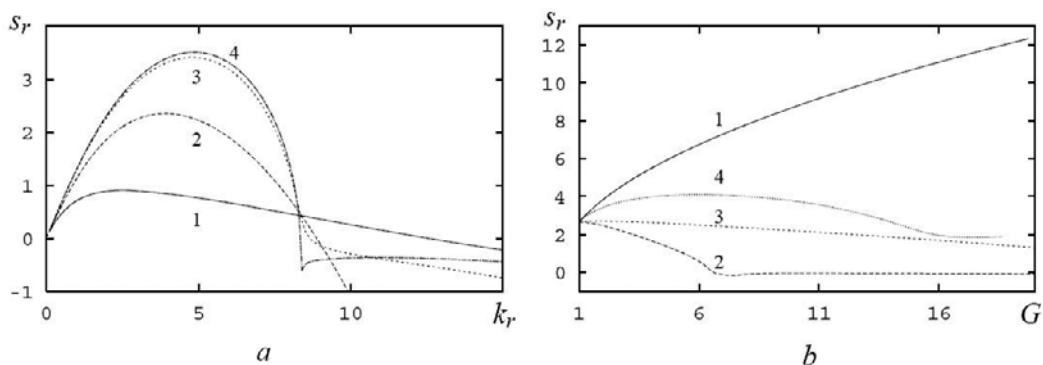


Figure 3. (a) Temporal amplification rate versus wavenumber for different Reynolds numbers. Curves 1–4 correspond to $Re=1, 10, 100, 800$. (b) Temporal amplification rate versus shear modulus $\Theta^{(j)}$ at $Re=100, k_r = 2.5$ for isotropic wall $\Theta_1^{(1)} = \Theta_2^{(1)} = \Theta_3^{(1)} = \Theta$ (curve 1), and anisotropic wall at $\Theta_{1,2}^{(2)} = \Theta_{1,2}^{(3)} = 1, \Theta_{1,2}^{(2)} = \Theta$ (curve 2), $\Theta_{1,2}^{(1)} = \Theta_{1,2}^{(3)} = 1, \Theta_{1,2}^{(2)} = \Theta$ (curve 3), $\Theta_{1,2}^{(1)} = \Theta_{1,2}^{(2)} = 1, \Theta_{1,2}^{(3)} = \Theta$ (curve 4).

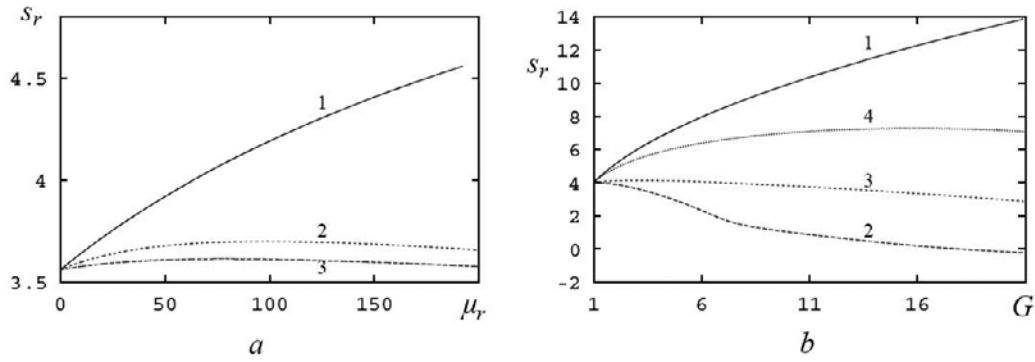


Figure 4. (a) Temporal amplification rate of the most-unstable mode versus the viscosity of one of the three isotropic layers, $\Theta_1^{(1)} = \Theta_1^{(2)} = \Theta_1^{(3)} = 1$ at $\mu_r^{(2)} = \mu_r^{(3)} = 0$ (curve 1), $\mu_r^{(1)} = \mu_r^{(3)} = 0$ (curve 2), and $\mu_r^{(1)} = \mu_r^{(2)} = 0$ (curve 3). (b) Temporal amplification rate versus shear modulus Θ for the viscoelastic layers at $\mu_r^{(1)} = \mu_r^{(2)} = \mu_r^{(3)} = 30$, for the isotropic wall $\Theta_1^{(1)} = \Theta_1^{(2)} = \Theta_1^{(3)} = \Theta$ (curve 1), and the anisotropic wall at $\Theta_1^{(2)} = \Theta_1^{(3)} = 1$, $\Theta_1^{(1)} = \Theta$ (curve 2), $\Theta_1^{(1)} = \Theta_1^{(3)} = 1$, $\Theta_1^{(2)} = \Theta$ (curve 3), and $\Theta_1^{(1)} = \Theta_1^{(2)} = 1$, $\Theta_1^{(3)} = \Theta$ (curve 4).

the third layers results in insignificant variation of the amplification rate, though the mode is slightly damped for the very viscous wall material. Increasing of the viscosity of the first layer that is in contact with the fluid significantly destabilizes the system. In other words, high viscosity of the first layer enhances the fluid–structure interaction and, consequently, the energy transfer from the fluid to the solid. It is worthy to note that when the no-displacement condition is applied to the outer surface, the viscosity of the second layer strongly stabilizes the system [20].

For the viscoelastic layers an increase in the shear modules $\Theta_1^{(3)} = \Theta_2^{(3)}$ of the outer layer leads to increasing the system instability (Fig. 4b) in contrast to the elastic wall while the stabilizing effect of the shear modulus of the inner layer is also observed at sufficiently high values $\Theta_1^{(1)} = \Theta_2^{(1)}$. The system stability and the behavior of the unstable modes are very sensitive to the material parameters of the layers, as it has been found by numerical computations within the wide limits of the thicknesses and viscoelastic parameters of the layers. The stabilizing effect of the inner layer has been observed in each case at $\Theta_1^{(1)} = \Theta_2^{(1)} < \Theta^*$ where the value Θ^* depends on the viscosity of the layer.

The amplification rate of the most-unstable mode versus the viscosity of each of the layers is plotted in Fig. 5a. The cases $\Xi_1^{(j)} = 20\Theta^{(j)}$, $\Xi_2^{(j)} = 2\Theta^{(j)}$ and $\Xi_1^{(j)} = 2\Theta^{(j)}$, $\Xi_2^{(j)} = 20\Theta^{(j)}$ have been considered. In each case, the viscosity of two layers is kept constant while the viscosity of the remained one varies. As can be seen, increasing the viscosity of the first layer, which is in contact with the fluid, leads to an increase of the amplification rate of the most-unstable mode (Fig. 5a). Thus, increasing the viscosity of the first layer destabilizes the system. The effect can probably be explained by better fluid–solid coupling when the viscosity of the inner layer is sufficiently high. The viscosity of the second layer shows a stabilizing effect (Fig. 5a), whereas the system is quite indifferent to variation of the viscosity of the third layer. There is no clear explanation of the surprising effect concerning the stabilizing effect of viscosity of the middle layer.

Owing to the fact that the viscosities of the first and second layers have an opposite effect, one cannot use Benjamin’s classification [46] in order to classify this mode in one of the classes noted A, B and C. In fact, according to Benjamin’s classification, if one considers the total disturbance energy of the coupled fluid–solid system, a decrease in that energy leads to destabilization of the modes of class A and to stabilization of the modes of class B, and has no effect on the modes of class C. The effect of the viscosity of the first (second, third) layers suggests that class A (B, C) is an appropriate one for the corresponding case. Consequently, this unstable mode could not belong to any of these classes. Note that the most-unstable mode is near the real axis, which suggests that the mode is a fluid-based one, and that the second unstable mode with small amplification rate is near the imaginary axis, which suggests that this is a solid-based mode [20].

The group velocity of the most-unstable mode versus the viscosity of the layers is presented in Fig. 5b. Note that when $\mu_r^{(2)} = 0$, the group velocity is negative. Therefore, it is all about an upstream-propagating wave. An increase in the viscosity of the first layer, which is in contact with the fluid, leads to an increase in the group velocity. In that way, the faster modes have higher viscosities. Variation of

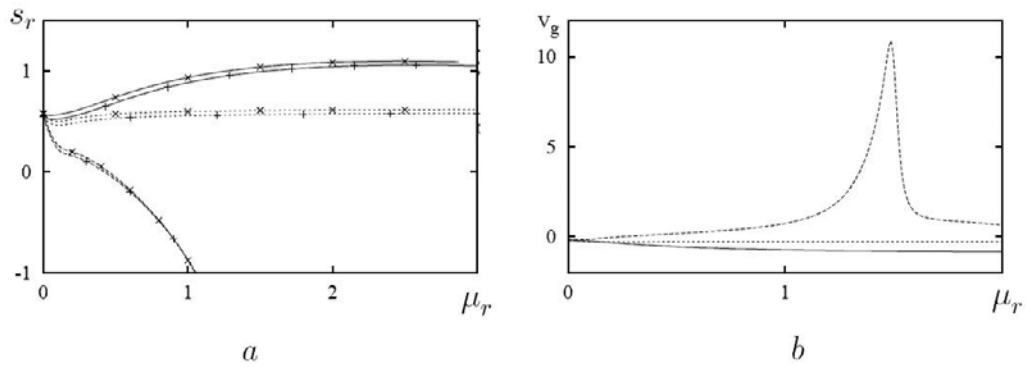


Figure 5. (a) Temporal amplification rate of the most-unstable mode versus the viscosity of the three anisotropic layers. The parameters of the system are $v_1^{(j)} = v_2^{(j)} = 0.1$. Solid line corresponds to $\mu_r^{(2)} = \mu_r^{(3)} = 0$; dashed line to $\mu_r^{(1)} = \mu_r^{(3)} = 0$, and dotted line to $\mu_r^{(1)} = \mu_r^{(2)} = 0$. The symbol + corresponds to $\Xi_1^{(j)} = 20\Theta^{(j)}$, $\Xi_2^{(j)} = 2\Theta^{(j)}$, symbol x to $\Xi_1^{(j)} = 2\Theta^{(j)}$, $\Xi_2^{(j)} = 20\Theta^{(j)}$. (b) Group velocity of the most-unstable mode versus the viscosity of the three anisotropic layers. $v_1^{(j)} = v_2^{(j)} = 0.1$, $\Xi_1^{(j)} = 20\Theta^{(j)}$, $\Xi_2^{(j)} = 2\Theta^{(j)}$. Solid line corresponds to $\mu_r^{(2)} = \mu_r^{(3)} = 0$, dashed line to $\mu_r^{(1)} = \mu_r^{(3)} = 0$, and dotted line to $\mu_r^{(1)} = \mu_r^{(2)} = 0$.

the viscosity of the third layer leads to a relatively insignificant alteration in the speed of propagation of the unstable mode. Surprisingly, any change in the viscosity of the middle layer leads to an inversion of the direction of the propagation of the unstable mode, where the group velocity becomes positive. For certain value of $\mu_r^{(2)}$, the group velocity is zero, which suggests the existence of absolute instability in the anisotropic, three-layer tube. The existence of such absolute instability in isotropic viscoelastic tubes has been shown in [18].

For tubes made of the same number of layers with the same rheological parameters, the system stability is different for the no-stress and no-displacement boundary condition cases. When the outer layer is attached to a rigid medium, the shear modules $\Theta_1^{(1)} = \Theta_2^{(1)}$ and $\Theta_1^{(2)} = \Theta_2^{(2)}$ produce quasi-opposite effects on the system stability. The amplification rate decreases but remains positive with increasing the shear modulus $\Theta_1^{(1)} = \Theta_2^{(1)}$. The amplification rate significantly increases with increasing the shear modulus $\Theta_1^{(2)} = \Theta_2^{(2)}$, whereas the value $\Theta_1^{(3)} = \Theta_2^{(3)}$ produces a relatively small increase in the amplification rate while the rest of the parameters, including the shear modulus of the two other layers, are kept constant and different. Variation of the shear modules $\Theta_{1,2}^{(1)}$ of the inner layer that is in contact with the fluid has also been found to exert great influence on the group velocity of the most-unstable mode. For sufficiently high values of $\Theta_{1,2}^{(1)}$, the disturbance changes its direction and becomes a downstream propagating wave.

For both types of boundary conditions, an increase in the shear modulus of the inner layer leads to stabilization of the system, although the effect is more pronounced for the no-displacement condition. When the outer layer is attached to a less-compliant medium, such as when a blood vessel is attached to surrounding tissues, the temporal amplification rate is scarcely affected by the shear modulus of the constrained layer. In contrast to the case of a constrained wall, the system can be stabilized by increasing the shear modulus of the third layer if displacement of the outer surface of the tube is allowed by the boundary condition.

Influence of anisotropy of the layers on the system stability has been investigated by calculating the temporal amplification rate of the most-unstable mode for the isotropic layers $\Xi_1^{(j)} = \Xi_2^{(j)}$ and when one of the layers is transversely isotropic and $\Xi_1^{(j)} \neq \Xi_2^{(j)}$. Some numerical results are presented in Figs. 6a–d. Simultaneous increase in the Young’s modules of all the layers (Fig. 6a), and of the inner (Fig. 6b), middle (Fig. 6c) and outer (Fig. 6d) layers separately is compared in each figure for isotropic and anisotropic materials.

Curve 1 in Fig. 6a is obtained by varying $\Xi_1^{(j)} = \Xi_2^{(j)} = \Xi, j = 1,2,3$, while the other parameters are hold constant. We observe a dramatic fall of the temporal amplification rate though the mode remains unstable. Increasing the parameters $\Xi_1^{(j)} = \Xi, j = 1,2,3$ leads to system stabilization, as shown by curve 2 in Fig. 6a, which is obtained by varying one of the parameters $\Xi_1^{(j)} = \Xi$ while other parameters are kept constant. When $\Xi \leq 8$, the most-unstable mode becomes stable. Increasing of the parameter $\Xi_2^{(j)} = \Xi$ for all the layers $j = 1,2,3$ leads to opposite effect and enhances the system instability. An increase in the

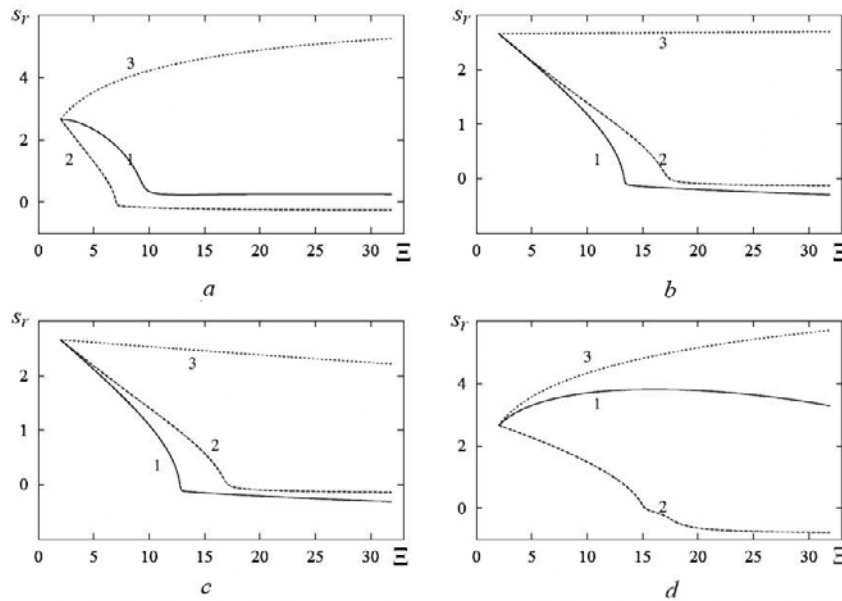


Figure 6. Temporal amplification rate of the most-unstable mode for anisotropic layers at different values of the Young's modules. (a) $\Xi_1^{(j)} = \Xi_2^{(j)} = \Xi$ (curve 1), $\Xi_1^{(j)} = \Xi_1$ (curve 2), $\Xi_2^{(j)} = \Xi$ (curve 3); (b) $\Xi_1^{(1)} = \Xi_2^{(1)} = \Xi$ (curve 1), $\Xi_1^{(1)} = \Xi$ (curve 2), $\Xi_2^{(1)} = \Xi$ (curve 3); (c) $\Xi_1^{(2)} = \Xi_2^{(2)} = \Xi$ (curve 1), $\Xi_1^{(2)} = \Xi$ (curve 2), $\Xi_2^{(2)} = \Xi$ (curve 3); and (d) $\Xi_1^{(3)} = \Xi_2^{(3)} = \Xi$ (curve 1), $\Xi_1^{(3)} = \Xi$ (curve 2), $\Xi_2^{(3)} = \Xi$ (curve 3).

Young's modules of the first, second and third layers separately influences the system stability in different ways, as is shown in Figs. 6b–d. The temporal amplification rate decreases noticeably with increasing $\Xi_1^{(1)} = \Xi_2^{(1)} = \Xi$ (curve 1 in Fig. 6b) and $\Xi_1^{(1)} = \Xi$ (curve 2 in Fig. 6b), and the system accordingly becomes stable at $\Xi_1^{(1)} < 13$ and $\Xi_1^{(1)} < 18$. Increasing the value $\Xi_2^{(1)}$ does not influence stability of the most-unstable mode.

Effect of changing the Young's modulus of the second layer is similar to the effect of Young's modulus of the first layer, as we may conclude from Fig. 6c. For the case $\Xi_1^{(2)} = \Xi_2^{(2)} = \Xi$ (curve 1 in Fig. 6c) and $\Xi_1^{(2)} = \Xi$ (curve 2 in Fig. 6c), stabilization of the system can be reached at approximately the same values $\Xi_1^{(1)} < 13$ and $\Xi_1^{(1)} < 18$.

Anisotropy of the third layer exerts the most significant influence, as is shown in Fig. 6d. An increase in $\Xi_1^{(2)}$ stabilizes the system, while an increase in $\Xi_2^{(2)}$ destabilizes it. When $\Xi_1^{(3)} = \Xi_2^{(3)} = \Xi$, the system remains unstable and the temporal amplification rate is approximately of the same order of magnitude as the mean temporal amplification rate obtained by independent variation of $\Xi_1^{(3)}$ and $\Xi_2^{(3)}$.

Based on the present results, optimal flow regimes (Reynolds number and forced frequency at inlet of the duct) as well as thicknesses and rheological parameters of the wall layers can be calculated for obtaining the appropriate stabilization conditions. In different transportation systems when maximum flow rate is an important factor and system stability is desired, the rigid outer layer and viscous middle layer should be chosen for, respectively, the no-stress and no-displacement boundary conditions at the outer surface of the tube. At certain flow conditions, mass and heat transfer at the fluid–solid interface or the rate of chemical reactions at the inner surface and within the liquid volume can be increased due to wall oscillations caused by system instability. The calculated results determine the set of material parameters of the tube and the appropriate flow regime for flow destabilization as well.

In that way the present numerical results reveal some novel opportunities for stabilization of fluid flow in transversely anisotropic, multilayered viscoelastic tube by a proper choice of the elastic and viscoelastic materials for the layers. In blood vessels, differences in $\Xi_1^{(j)}$ and $\Xi_2^{(j)}$ are connected with wall structure. Each layer is composed of a set of the sheets (laminas) with different material parameters, while connection between the sheets (in the radial direction) is provided by the fibers, which are usually more extensible and flexible than the fibers located in the sheets in the plane of isotropy of the layers. The difference is most important for the middle layer composed of several elastic laminas attached to each other by elastic fibers. In technical materials, anisotropy is determined by orientation of the

polymer chains, grains and other inclusions, and by orientation of the fibers in fiber-reinforced composites.

4. CONCLUSIONS

Stability analysis of a steady flow in thin- and thick-walled uniform and multilayered viscoelastic tubes revealed some ways to increase the system stability by targeting the most-unstable modes. It was shown that the system instability strongly depends on the rheological properties of the wall. Shear moduli and viscosities of the layers produce the most prominent effects on the temporal and spatial amplification rates and on the group velocity of the unstable mode. When the compliant tube is composed of three layers with the same material parameters (a single-layer, thick-walled tube), the system is found to be unstable. When the material parameters of the layers are different, the system may possess lower temporal amplification rates and can become stable.

An increase in the shear modulus of the inner and middle layers decreases the temporal amplification rate and stabilizes the system whereas some increase in rigidity of the outer layer eliminates the temporal instability of a steady viscous flow in a compliant tube. Comparative analysis of system stability at the no-displacement and no-stress boundary conditions at the outer surface of the duct revealed that stabilization of the system can be achieved in both cases by increasing the rigidity of the inner layer. For a transversely anisotropic material, temporal stability can be achieved by increasing the shear modulus in the plane of isotropy of any of the layers at the no-stress boundary condition, and by increasing the viscosity of the second layer at the no-displacement condition.

The present results point to a novel strategy to eliminate flow-induced wall vibrations and to stabilize a fluid flow through a compliant tube by carefully choosing the values of the shear moduli and viscosities of the different layers. In that way optimal parameters of a composite wall that provide system stabilization can be chosen to construct sound absorption and vibration damping coatings in aerospace vehicles and noise-generating devices. As applied to biomedical problems, the present results shed new light on the stability/instability of blood vessels at the pathology connected with wall thickening and the corresponding interrelated variations of the viscosities, elastic coefficients and densities of the layers. The computed multilayered compliant coatings can be used for flow control in different ducts conveying fluid. Based on the theory presented, the calculated results can be generalized for non axisymmetric disturbances, which also take place in tubes of both technical devices and blood vessels.

ACKNOWLEDGEMENTS

This work is partially supported by NASU-CNRS PICS 2008–2010 grant for international cooperation.

REFERENCES

1. J.B. Grotberg, and O.E. Jensen, Biofluid mechanics in flexible tubes, *Annual Review of Fluid Mechanics*, 2004, 36, 121–147.
2. T.J. Pedley, Longitudinal tension variation in collapsible channels: a new mechanism for the breakdown of steady flow, *ASME J. of Biomechanical Engineering*, 1992, 114, 60–67.
3. T.J. Pedley, and X.Y. Luo, Modelling flow and oscillations in collapsible tubes, *Theoretical and Computational Fluid Dynamics*, 1998, 10, 277–294.
4. W.A. Conrad, Pressure-flow relationships in collapsible tubes, *IEEE Transactions BME*, 1969, 16, 284–295.
5. A.H. Shapiro, Steady flow in collapsible tubes, *J. of Biomechanical Engineering*, 1977, 99, 126–147.
6. M. Gad-el-Hak, Drag reduction using compliant walls, in *Flow Past Highly Compliant Boundaries and in Collapsible Tubes* (eds. P. W. Carpenter and T. J. Pedley), Kluwer, 2003, 191–230.
7. R. Kadoli, and N. Ganesan, Parametric resonance of a composite cylindrical shell containing pulsatile flow of hot fluid, *Composite Structures*, 2004, 65, 391–404.
8. M.O. Kramer, Boundary-layer stabilization by distributed damping, *J. of American Society of Navigation Engineers*, 1960, 72, 25–33.

9. M. Gad-el-Hak, Compliant coatings – a decade of progress, *Applied Mechanics Reviews*, 1996, 49, S147–S157.
10. K.S. Choi, X. Yang, B.R. Clayton, E.J. Glover, M. Atlar, B.N. Semenov, and V.M. Kulik, Turbulent drag reduction using compliant surfaces. *Proc. of the Royal Society London, Ser. A*, 1997, 453, 2229–2240.
11. P.W. Carpenter, C. Davies, and A.D. Lucey, Hydrodynamics and compliant walls: Does the dolphin have a secret? *Current Science*, 2000, 79, 758–765.
12. P.W. Carpenter, Status of transition delay using compliant walls, in *Viscous drag reduction in boundary layers*, (eds. D. M. Bushnell, and J. N. Hefner), AIAA, 1990, 79–113.
13. J.J. Riley, M. Gad-El-Hak, and M. Metcalfe, Compliant coatings, *Annual Review of Fluid Mechanics*, 1988, 20, 393–420.
14. P.W. Carpenter, and A.D. Garrad, The hydrodynamic stability of flows over Kramer-type compliant surfaces. Part 2. Flow-induced surface instabilities, *J. of Fluid Mechanics*, 1986, 70, 199–232.
15. P.W. Carpenter, Optimization of multiple-panel compliant walls for delay of laminar-turbulent transition, *AIAA Journal*, 1993, 31, 1187–1188.
16. M. Gaster, Is the dolphin a red herring?, *Proc. IUTAM Symp. on Turbulence Management and Relaminarisation*, (eds. H. W. Liepmann and R. Narasimha), Springer, 1987, 285–304.
17. A.D. Lucey, P.W. Carpenter, and A.E. Dixon, The role of wall instabilities in boundary layer transition over compliant walls, *Proc. Boundary Layer Transition and Control*, Cambridge, Royal Aeronautical Society, 1991, 35, 1–35.
18. M. Hamadiche, and M. Gad-el-Hak, Temporal stability of flow through viscoelastic tubes, *J. of Fluids and Structures*, 2002, 16, 331–359.
19. M. Hamadiche, and M. Gad-el-Hak, Spatiotemporal stability of flow through collapsible, viscoelastic tubes, *AIAA Journal*, 2004, 42, 772–786.
20. M. Hamadiche, and N. Kizilova, Temporal and spatial instabilities of the flow in the blood vessels as multi-layered compliant tubes, *Intern. J. of Dynamics of Fluids*, 2005, 1, 1–23.
21. M. Hamadiche, and N. Kizilova, Flow interaction with composite wall. In: *ASME Conference 'Pressure Vessels and Piping'*, Vancouver, 2006, PVP2006-ICPVT11-93880.
22. M. Hamadiche, N. Kizilova, and M. Gad-el-Hak, Suppression of absolute instabilities in the flow inside a compliant tube, *Communications in Numerical Methods in Engineering*, 2009, 25, 505–531.
23. N. Banerjee, and P. Jayakumar, Compliant materials for drag reduction of high-speed submerged bodies, *Defence Science Journal*, 2005, 55, 37–42.
24. V.V. Pavlov, Dolphin skin as a natural anisotropic compliant wall, *Bioinspiration and Biomimetics*, 2006, 1, 31–40.
25. R.Z. Grosskreut, An attempt to control boundary-layer turbulence with non-isotropic compliant walls, *University Science J.*, 1975, 1, 67–72.
26. P.W. Carpenter, and P.J. Morris, The hydrodynamic stability of flows over non-isotropic compliant surfaces—Numerical solution of the differential eigenvalue problem, in *Numerical Methods in Laminar and Turbulent Flows*, Pineridge, 1985, 1613–1624.
27. P.W. Carpenter, and A.D. Garrad, The hydrodynamic stability of flows over Kramer-type compliant surfaces. Part 1. Tollmien–Schlichting instabilities, *J. Fluid Mechanics*, 1985, 155, 465–510.
28. N. Kizilova, and M. Hamadiche, Stability analysis of blood flow in multilayered viscoelastic tubes, *Computer Methods in Biomechanics and Biomedical Engineering*, 2005, Suppl.1, 165–166.
29. N. Kizilova, and M. Hamadiche, Stability of the fluid flows past deformable surfaces, in *Collapsible Tubes and Channels*, *Kharkov National University Vestnik*, 2007, 790, 53–82.
30. R. Rosen, *Optimality Principles in Biology*, Plenum Press, NY, 1967.
31. M. La Barbera, Principles of design of fluid transport systems in zoology, *Science*, 1990, 249, 992–1000.

32. N. Kizilova, and N. Popova, Investigation of the transport systems of leaves, *Problems of Bionics*, 1999, 51, 71–79.
33. N. Kizilova, Computational approach to optimal transport network construction in biomechanics, *Lecture Notes in Computer Sci.*, 2004, 3044, 476–485.
34. N. Kizilova, Long-distance liquid transport in plants, *Proceedings of Estonian Academy of Sciences, Ser. Physics and Mathematics*, 2008, 57, 179–203.
35. W. Zhi, Zh. Ming, and Y. Qi-Xing, Modeling of Branching Structures of Plants, *J. Theoretical Biology*, 2001, 209, 383–394.
36. D.B. Chklovskii, and A. Stepanyants, Power-law for axon diameters at branch point, *BMC Neuroscience*, 2003, 4, 18–25.
37. J.D. Hartman, Structural changes within the media of coronary arteries related to intimal thickening, *American J. of Pathology*, 1977, 89, 13–34.
38. Y.-J. Zhuang, T.M. Singh, C.K. Zarins, and H. Masuda, Sequential increases and decreases in blood flow stimulates progressive intimal thickening, *European J. of Vascular and Endovascular Surgery*, 1998, 16, 301–310.
39. J. Lighthill, *Mathematical biofluidynamics*, Philadelphia, Society for Industrial and Applied Mathematics, 1975.
40. Y.C. Fung, *Biomechanics: Circulation*, Springer-Verlag, New York, 1996.
41. M. Gad-el-Hak, *Flow control. Passive, active and reactive flow management*, Cambridge University Press, 2000.
42. H. Alderson, and M. Zamir, Smaller, stiffer coronary bypass can moderate or reverse the adverse effects of wave reflections, *J. Biomechanics*, 2001, 34, 1455–1462.
43. T. Frauenfelder, E. Boutsianis, T. Schertler, L. Husmann, S. Leschka, D. Poulidakos, B. Marincek, and H. Alkadhi, Flow and wall shear stress in end-to-side and side-to-side anastomosis of venous coronary artery bypass grafts, *Biomedical Engineering Online*, 2007, 6, 35.
44. M. Johnson, and J.M. Tarbell, A biphasic, anisotropic model of the aortic wall, *Transactions of ASME*, 2001, 123, 52–57.
45. R.P. Vito, and S.A. Dixon, Blood vessel constitutive models—1995–2002, *Annual Review of Biomedical Engineering*, 2003, 5, 413–439.
46. T.B. Benjamin, The threefold classification of unstable disturbances in flexible surfaces bounding inviscid flows, *J. of Fluid Mechanics*, 1963; 16,43–50.

